Quaternary Research (2018), 1–15

doi:10.1017/qua.2018.81

New age controls on the tephrochronology of the southernmost Andean Southern Volcanic Zone, Chile

DJ Weller[a]*, ME de Porras[b], A Maldonado[c,d], C Méndez[e], CR Stern[a]

[a]Department of Geological Sciences, University of Colorado, Boulder, Colorado 80309-0399, USA
[b]Instituto Argentino de Nivología, Glaciología y Ciencias Ambientales (IANIGLA), CONICET, CCT Mendoza, Av. Ruiz Leal s/n, Mendoza, Argentina
[c]Centro de Estudios Avanzados en Zonas Áridas (CEAZA), Instituto de Investigación Multidisciplinario en Ciencia y Tecnología, Universidad de La Serena, Avda. Raúl Bitrán 1305, La Serena, Chile
[d]Departamento de Biología Marina, Universidad Católica del Norte, Larrondo 1281, Coquimbo, Chile
[e]Centro de Investigación en Ecosistemas de la Patagonia (CIEP), Moraleda 16, Coyhaique, Chile

(Received February 26, 2018; Accepted June 27, 2018)

Abstract

The chronology of over 50 tephra layers preserved in a lake sediment core from Laguna La Trapananda (LLT) in the southern portion of the Andean Southern Volcanic Zone (SSVZ), Chile, is constrained by new radiocarbon age determinations, which span the period from late Pleistocene glacial retreat to the late Holocene. The tephra are correlative with tephra previously described from other lake cores in the region and are attributed to explosive eruptions of the SSVZ volcanoes Mentolat, Hudson, Macá, and potentially Cay. The new age determinations are used to estimate the ages of the >50 tephra in the LLT core, as well as those from the other previously described lake cores in the area, by a Bayesian statistical method. The results constrain the frequency of explosive eruptions of the volcanic centers in the southernmost SSVZ. They indicate that there was essentially no increase in the rate of eruptions from late-glacial to recent times due to deglaciation. They also provide isochrones used to constrain the depositional histories of the small lacustrine systems within which they were deposited and they provide a tephrochronologic tool for other paleoclimatic, paleoecologic, archaeologic and tephrochronologic studies in central Patagonia.

Keywords: volcanism; tephra; tephrochronology; Andes; Patagonia; Chile

INTRODUCTION

Lakes and bogs from the southern portion of the Andean Southern Volcanic Zone (SSVZ; Fig. 1) preserve exceptional records of late-glacial and Holocene explosive volcanism because of their nearly continuous record of sedimentation since glacial retreat, which allows for the preservation of tephra from both small and large explosive eruptions (Stern et al., 2016, 2015, Weller et al., 2017, 2015, 2014). The detail of these tephra records are unrivaled by subaerial soil sequences, which rarely contain records with the same exceptional stratigraphic control observed in lake sediment cores. Once tephra layers are characterized geochemically and lithostratigraphically, they can be correlated with one another in sediment cores or subaerial tephra exposures over a wide region and used as time-synchronous horizons, which can be important for linking regional paleoclimatic, archaeologic, and geologic archives (Fontijn et al., 2016, 2014; Lowe, 2011). Detailed tephrochronologic studies from north in the Andean SVZ near Chaitén and Minchinmávida, (Alloway et al., 2017b, 2017a; Watt et al., 2011b), and Mocho-Choshuenco (Rawson et al., 2015), which are based primarily on subaerial tephra exposures, and others based on lacustrine sedimentary records (Bertrand et al., 2008; Daga et al., 2016), have identified and correlated both small and large eruptions and have provided important information on the rate and magnitude of eruptions from the SVZ centers since glacial retreat.

A sediment core taken from the small Laguna La Trapananda (LLT; Fig. 1), which has a limited internally drained catchment size of less than 2 km^2, preserves over 50 tephra layers (Fig. 2) derived from explosive eruptions of volcanoes of the southernmost portion of the Andean Southern Volcanic Zone (SSVZ). Based on both their stratigraphic positions within the cores, bulk tephra geochemistry, and their petrology (mineralogy and glass morphology and color; Table S1

*Corresponding author at: Department of Geological Sciences, University of Colorado, Boulder, Colorado 80309-0399, USA. E-mail address: derek.weller@colorado.edu (D.J. Weller).

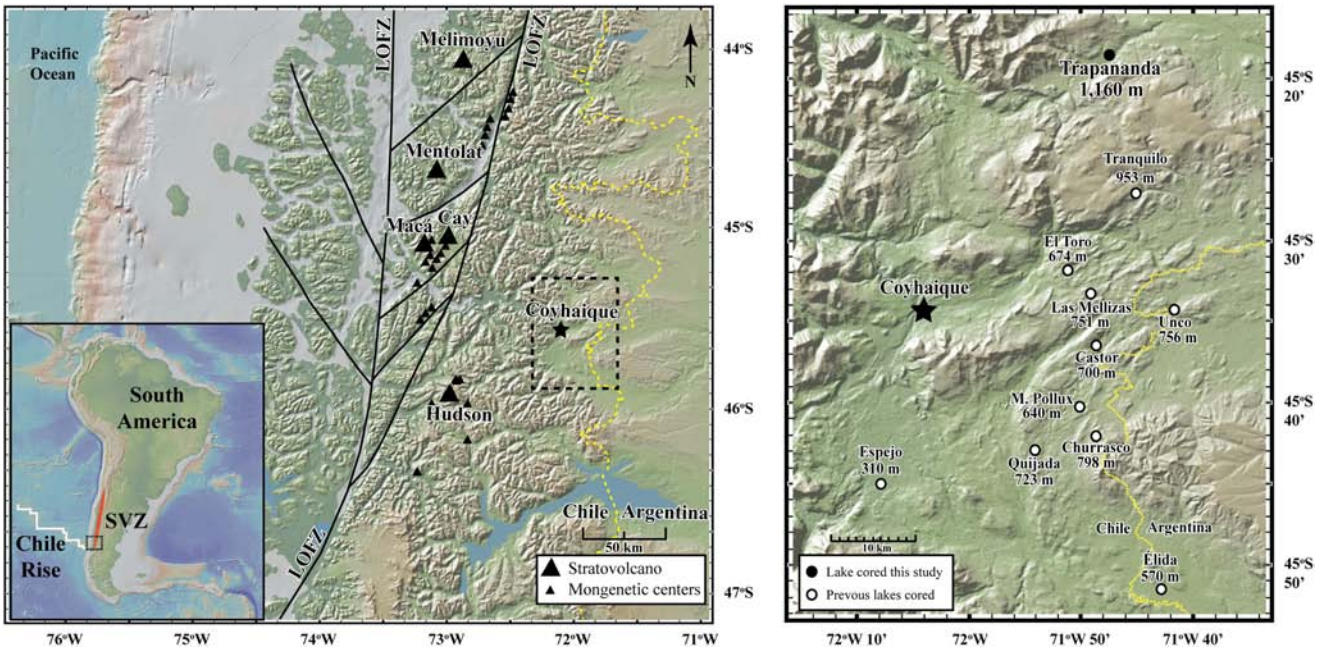

Figure 1. (color online) Map (on the left) of the southernmost portion of the Andean SVZ showing the location of the major volcanoes and some of the minor monogenetic eruptive centers (MEC) along the Liquiñe-Ofqui Fault Zone (LOFZ) and surrounding Hudson, Macá and Cay (D'Orazio et al., 2003; Gutiérrez et al., 2005; López-Escobar et al., 1995a; Vargas et al., 2013). The dashed box shows the area of the map (on the right) locating Laguna La Trapananda (LLT; solid circle) and the other lakes (open circles) from which sediment cores have been extracted and tephra identified near Coyhaique (Elbert et al., 2013; Weller et al., 2015). Also indicated is the location of Mallín el Pollux (Markgraf et al., 2007), and the altitude above sea level in meters of each of the lakes. Map constructed using GeoMapApp (http://www.geomapapp.org).

of the supplementary material), most of the tephra from this lake can be correlated to those in other previously described lake sediment cores located 15-57 km to the south (Figs. 1 and 3; Weller et al., 2015).

The ages of the tephra in the LLT core have been constrained by seven new radiocarbon dates (Table 1). Based on these new age determinations, the ages of the >50 tephra from Laguna La Trapananda, as well as tephra from the other lake sediment cores in the area for which there was previously only limited chronological control, have then been estimated by Bayesian age modeling using the OxCal program with the Southern Hemisphere radiocarbon calibration data (SM1 of the supplementry material; Hogg et al., 2013). The results provide a refined tephrochronology, with significantly more robust internal constraints, for the multiple tephra produced by explosive eruptions of the volcanoes of the Andean SSVZ. These data are useful for determining the recurrence frequency of explosive eruptions of SSVZ volcanoes and the sedimentation rates in the lakes from which the cores were obtained, which may or may not reflect the timing of paleoclimate variations from the late-glacial to the present time in this region of Patagonia.

BACKGROUND

The Andean SVZ (inset Fig. 1) consists of ~70 Pleistocene and Holocene composite stratovolcanoes, as well as numerous minor monogenetic eruptive centers (MEC; Stern, 2004). This 1400 km long volcanic chain has been divided into a Northern (NSVZ; 33°S-34.5°S), Transitional SVZ (TSVZ; 34.5°S-37°S), Central SVZ (CSVZ; 37°S-41.5°S) and southernmost (SSVZ; 41.5°S-46°S) sections based on the geometry of the arc (Völker et al., 2011).

The petrogenesis and eruptive histories of the volcanoes of the southernmost SSVZ are of interest because of their location in close proximity to the subduction of the Chile spreading ridge (see inset in Fig. 1; D'Orazio et al., 2003; Futa and Stern, 1988; Gutiérrez et al., 2005; Kratzmann et al., 2010, 2009; López-Escobar et al., 1993; Vargas et al., 2013). This study focuses on tephra produced by explosive eruptions of the volcanoes of the southernmost part of the SSVZ, which consists of the five large volcanoes Melimoyu, Mentolat, Macá, Cay, and Hudson (Fig. 1), as well as many minor eruptive centers (MEC) located both around the major volcanoes and along the Liquiñe-Ofqui Fault Zone (Fig. 1; LOFZ; D'Orazio et al., 2003; Gutiérrez et al., 2005; López-Escobar et al., 1995, 1993; Vargas et al., 2013).

Previous tephrochronologic studies in the SSVZ have relied both on lithostratigraphic data (age, tephra grain size, glass color and morphology, mineralogy, etc.), as well as geochemical differences (bulk tephra and glass shard compositions), to correlate tephra observed in lake and ocean sediment cores amongst themselves and to other tephra described in outcrop (Carel et al., 2011; Elbert et al., 2013; Haberle and Lumley, 1998; Naranjo and Stern, 2004; Stern et al., 2016, 2015, Weller et al., 2017, 2015, 2014). These studies have demonstrated that, in this region of the Andean SSVZ, tephra derived from different source volcanoes, as determined by isopach maps of their

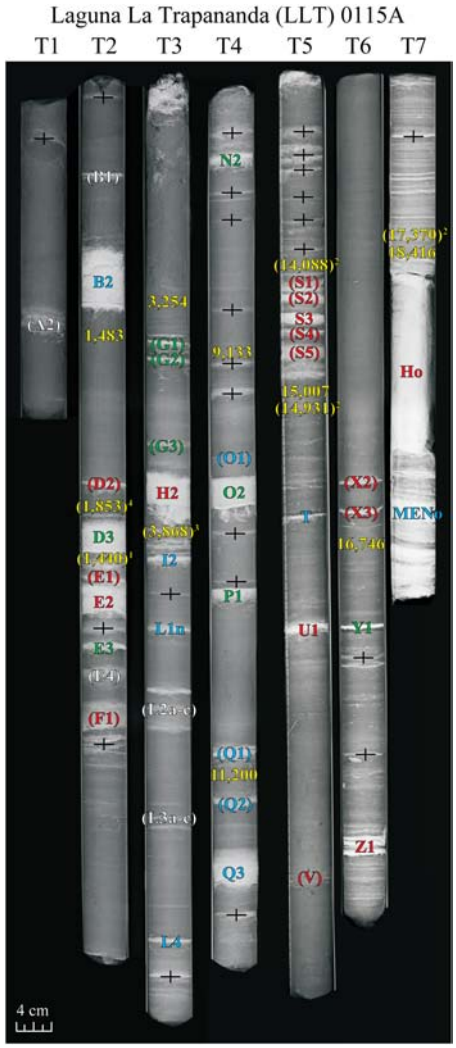

Figure 2. (color online) Transmitted X-ray images of the lake sediment core from Laguna La Trapananda (LLT). The tephra in this core appear as white layers due to their higher density compared to the predominantly organic lake sediments in which they are preserved. Sampled and unsampled (in parentheses) tephra that have been correlated with tephra in other lake sediment cores from near Coyhaique are labeled with the same nomenclature used in Weller et al. (2015), and numerous thin unsampled dense layers, most probably tephra, are indicated by a plus (+) symbol. The tephra labels have been color coded according to the source volcano (red tephra from Hudson, blue from Mentolat, and green from either Macá, Cay, or a monogenetic eruptive centers). Tephra with white labels were not sampled from either the LLT core or the other cores from near Coyhaique, but are correlated based on stratigraphic relations. New and previously published (in parentheses: 1. Naranjo and Stern, 2004; 2. Weller et al., 2015; 3. Naranjo and Stern, 1998; 4. Elbert et al., 2013) radiocarbon age dates are shown in yellow.

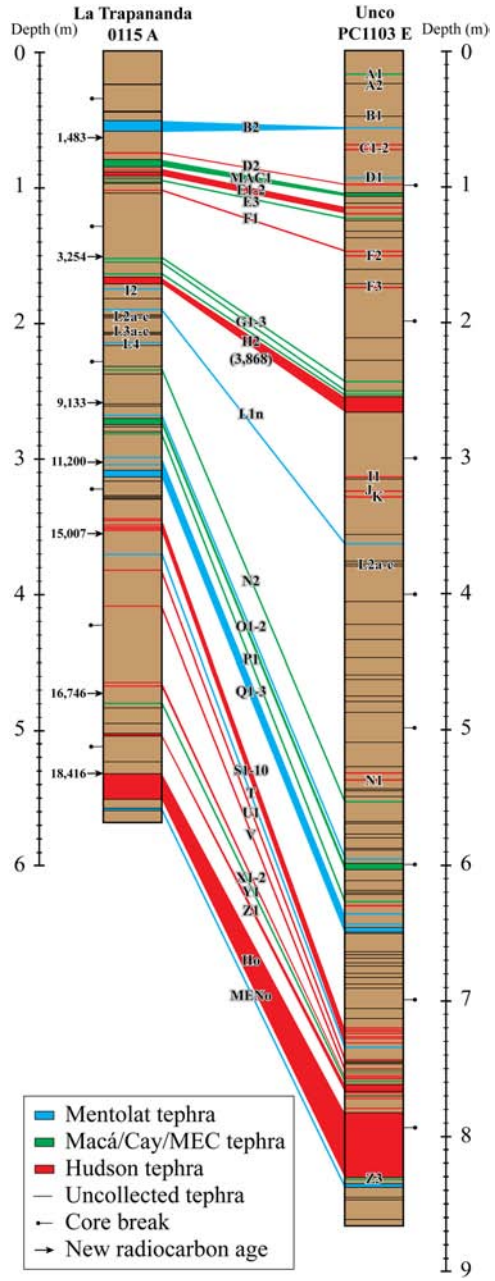

Figure 3. (color online) Stratigraphic columns and correlation of 39 tephra deposits in the Laguna La Trapananda (LLT) lake sediment core with those in a core from Unco lake (Fig. 1) located ~25 km south of LLT. The tephra in the Unco lake core have been described in detail and correlated with tephra from other lake sediment cores in the region by Weller et al. (2015). The new radiometric ages (in cal yr BP; Table 1) for the LLT core are indicated, as is the previously published age for the H2 tephra from Naranjo and Stern (1998).

relative thickness in relation to their distance from their source volcano, have significantly and consistently different bulk tephra geochemistry (Fig. 4), mineralogic and tephra glass characteristics (Fig. 5). These same criteria, as described in detail below, are also used here, where correlation with tephra in previously described lake sediment cores (Fig. 3) is done by comparing the stratigraphic relations of mineralogically, texturally, and geochemically distinct eruptions.

Concerning their whole rock geochemical characteristics, (López-Escobar et al., 1995a, 1993) classified the basalt of the Andean SVZ into two geochemical groups, termed Type-1 and Type-2, distinguished by the relative abundance K_2O and incompatible trace elements such as large ion-lithophile

Table 1. Radiocarbon age dates from Laguna La Trapananda.

Laboratory No.	Core	Section	Depth (cm)	^{14}C yr BP	1σ error	cal yr BP	1σ error
D-AMS 013305	0115A	AT2	28-29	1636	29	1483	39
D-AMS 017342	0115A	AT3	24-25	3082	22	3245	56
D-AMS 017343	0115A	AT4	28-29	8229	38	9133	76
D-AMS 017344	0115A	AT4	78-79	9804	38	11,200	45
D-AMS 013304	0115A	AT5	34-35	12,668	47	15,007	128
D-AMS 017345	0115A	AT6	53-54	13,878	43	16,746	124
D-AMS 013303	0115A	AT7	17-18	15,192	59	18,416	98

elements (LILE; Rb, Cs, Ba, Y, Th, and U), high-field strength elements, (HFSE; Ti, Zr, Hf, Ta) and rare earth elements (REE). Among the volcanoes of the SSVZ, Hudson, and Melimoyu have produced lavas and tephra with relatively high concentrations of incompatible trace elements such as LILE, HFSE and REE, and have been termed High Abundance (HA) geochemical types (Fig. 4; Stern et al., 2016, 2015; Weller et al., 2015) that correspond to the Type-2 chemical classification of López-Escobar et al. (1995a, 1993). Mentolat, Macá, Cay and the MEC have produced lavas and tephra that have relatively low concentrations of LILE, HFSE and REE (Fig. 4), which have been termed Low Abundance (LA) geochemical types and correspond to the Type-1 chemical classification of López-Escobar et al. (1995a, 1993).

A further division among the Type-1 or LA type centers has been made to distinguish the eruptive products from Mentolat, which produces amphibole-bearing andesitic and dacitic lavas and tephra with unusually low concentrations of LILE, HFSE and REE (Fig. 4), and has been termed a Very Low Abundance (VLA) or Low Abundance Felsic (LAF) geochemical type center (Stern et al., 2016, 2015; Weller et al., 2015). Mentolat is similar to some other centers in the SVZ such as Nevado de Longaví (Rodríguez et al., 2007; Sellés et al., 2004), Huequi (Watt et al., 2011a), and Calbuco (López-Escobar et al., 1995b), which also have erupted amphibole-bearing products with VLA type chemistry.

The volcanoes of the SSVZ also produce texturally and mineralogically distinct eruptive products that have been used as well to distinguish between the eruptions from the SSVZ centers (Stern et al., 2016, 2015, Weller et al., 2017, 2015, 2014). Specifically, Hudson tephra, including the H2 tephra (Fig. 5), Ho tephra (Weller et al., 2014) and others that are thickest in cores just east of the Hudson volcano, are all HA geochemical type that are light brown in color with tan pumice clasts and varying proportions of dark mafic components (Fig. 5A). Hudson eruptions are generally dominated by intermediate (basaltic andesite, andesite and dacite; Kratzmann et al., 2009; Stern et al., 2016; Weller et al., 2014, 2015) pale tan, microlite-free, highly elongated vesicle-rich glass (Fig. 5C), with orthopyroxene and plagioclase phenocrysts, and less commonly olivine and clinopyroxene, but without amphibole. However, other more mafic tephras containing less felsic material than the H2 tephra have also been attributed to eruptions of Hudson. These more mafic eruptions are darker brown in color and contain abundant plagioclase, clinopyroxene, and olivine with a smaller proportion of orthopyroxene. The tephra glass is dark brown, orange, or black in color with vesicles that are either circular or weakly deformed and varying amounts of mineral microlites. These tephra are similar texturally and mineralogically to mafic tephra derived from the other SSVZ centers but they can be distinguished by their HA character (Fig. 4).

In contrast, Mentolat tephra, including the Q3 eruption (Fig. 5) and others that are thickest just east of the Mentolat volcano in the Río Cisnes valley (Weller et al., 2017), are all VLA geochemical type tephra (Fig. 4) that are light grey to dark grey in color with clasts of white pumice and a small proportion of dark mafic components (Fig. 5D). Mentolat derived tephra contain abundant amphibole, orthopyroxene and plagioclase, as well as minor olivine and clinopyroxene (Fig. 5E), along with clear rhyolitic (Stern et al., 2016) glass containing abundant rounded vesicles and lacking mineral microlites (Fig. 5F). However, other more mafic eruptions of Mentolat have also been observed which contain a higher proportion of the dark mafic components and less white felsic pumice. These tephra also contain abundant plagioclase, orthopyroxene, clinopyroxene, amphibole, and olivine with black volcanic glass that lack identifiable vesicles or microlites. These eruptions can be distinguished from the other more mafic eruptions derived from the other volcanos of the SSVZ by the relatively high proportion of amphibole phenocrysts and the presence of white pumice glass with circular vesicles, and the VLA-type geochemistry (Fig. 4).

Tephra produced by eruptions of Macá, Cay and/or the small MEC in the region have a LA type geochemistry (Fig. 4) are all generally similar petrologically to the MAC1 eruption of Macá (Naranjo and Stern, 2004), which is dark brown to black in color with clasts of black scoria and dark brown pumice (Fig. 5G). Phenocrysts include abundant plagioclase, clinopyroxene and variable amounts of olivine, with minor orthopyroxene, and in a few instances trace amphibole (Fig. 5H). The tephra glass from the MAC1 eruption is diverse, with a portion of the glass being dark brown in color that is vesicle-poor with variable amounts of mineral microlites. A second type of glass is common in the MAC1 eruption and the other LA-type tephra which is black in color which lacks visible vesicles or microlites (Fig. 5I).

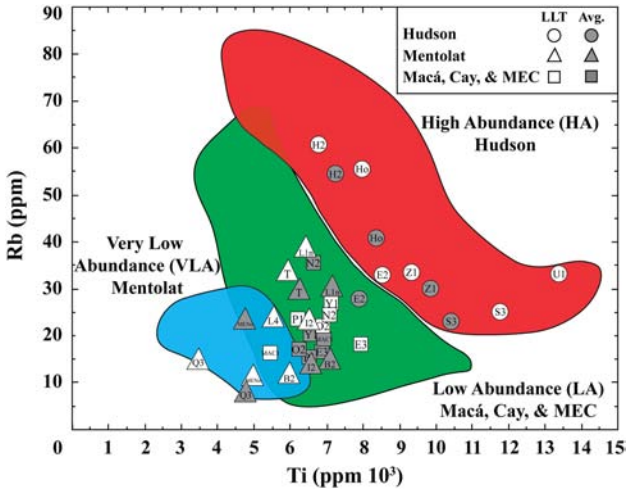

Figure 4. (color online) Ti versus Rb concentrations, in parts-per-million (ppm) illustrating the High Abundance (HA), Low Abundance (LA), and Very Low Abundance (VLA) compositional fields for SSVZ centers created using published data of lavas and tephra derived from Hudson, Mentolat, Macá, Cay and MEC (D'Orazio et al., 2003; Futa and Stern, 1988; Gutiérrez et al., 2005; López-Escobar et al., 1995a, 1993, Naranjo and Stern, 1998, 2004, Stern et al., 2016, 2015; Weller et al., 2014), bulk tephra from this study (labeled white symbols; Table 2, 3 and 4), and the average trace element content of the correlated terpha (labeled grey symbols) from other lake cores from near Coyhaique (Weller et al., 2015). The Hudson samples are all High Abundance (HA) petrochemical types, which contain generally higher Ti and Rb, than both the Low Abundance (LA) samples from Macá, Cay and MEC, and the Very Low Abundance (VLA) samples from Mentolat.

Tephra produced by explosive eruptions of Melimoyu, the northernmost volcano in this section of the SSVZ, have been documented to the east of this volcano (Naranjo and Stern, 2004; Stern et al., 2015; Weller et al., 2017), but not to the south near Coyhaique (Weller et al., 2015). No tephra derived from Melimoyu or any other volcano further north in the SSVZ occur among the tephra sampled in the LLT core, and all the >50 tephra in this core can be correlated with others produced by Mentolat, Macá, Cay and/or Hudson volcano in the previously described cores from the area (Figs. 3 and S1-S8 of the supplementary material; Weller et al., 2015). If any tephra produced by explosive eruptions of volcanoes further to the north occur in any of these cores, they only occur among the many thin unsampled tephra deposits in each core.

METHODS

The ~6 m long Laguna La Trapananda (LLT) sediment core (Fig. 2) was obtained using a modified piston corer (Wright, 1967). This lake, located 1,160 masl at 45°20'22.85"S and 71°50'11.49"W (Fig. 1), was selected because of its small size (<0.1 km^2) and limited basin catchment (<2 km^2) to reduce the amount of clastic input into the lacustrine system. The core was extracted at 1-meter intervals until the sediments transitioned from predominately organic-matter-rich lacustrine sediments to fine-grained glaciolacustrine sands and clays. The core was photographed using transmitted x-rays to aid in the identification of the tephra (Fig. 2). The dark material in the photo is the less dense organic matter rich lacustrine sediments and the white layers are the denser lithologies, which are often tephra deposits except in the deepest parts of the cores where fine-grained glaciolacustrine sands and clays occur.

The >50 tephra in the LLT core can in almost all cases be correlated (Fig. 3), based simply on their stratigraphic position, with the tephra in the other lake cores (Fig. 1 and S1-S8 of the supplementary material) previously described from the Coyhaique area by Weller et al. (2015). The A to Z nomenclature used for tephra in these other lacustrine sediment cores has also been used for the tephra in this new core (Figs. 2 and 3). For the nomenclature assignment, the youngest tephra which occur near the top of the sedimentary sequence and correspond to those previously described from the region (Weller et al., 2015) are named tephra A, while the oldest tephra that occur at the base of the lacustrine cores are named tephra Z. In some cases, groups of tephra occur in close spatial relation and were named for example, tephras E1-E4 and S1-S10, but all tephras within those groups may not have the same source volcanoes.

To further confirm these correlations, and to characterize some of the tephra only observed in the LLT core, a portion of 19 selected tephra were sampled from the core using a knife. These samples were washed in water and acetone to remove organic matter. A part of the cleaned sample was powdered in a moly-tungsten shatter box and dissolved in a mixture of HF, HNO_3 and HCl for trace element analysis using an ELAN D CR ICP-MS. Based on repeat analysis of internal standards with known compositions (Saadat and Stern 2011), these analyses are accurate to ±10% at the concentration levels in these tephra. Another part of the cleaned sample was mounted on a petrographic slide to describe features such a tephra glass color, vesicle morphology, microlite type and abundance, as well as the presence and identity of mineral phenocrysts (Table S1 of the supplementary material).

Seven AMS radiocarbon ages (Table 1) were determined, by DirectAMS Radiocarbon Dating Services (Brothwell, Washington, USA), on organic matter in bulk sediment samples within the core. The samples were portioned, treated with acids and a base, and converted to CO_2 by combustion of the organic matter which was then reduced to graphite. Carbon isotopes were measured on the NEC Pelletron 500 kV Accelerator Mass Spectrometer. Radiocarbon age dates were converted to calendar years before present (cal yr BP) by applying the ShCall 13 curve (Hogg et al., 2013) to the CALIB 7.0.4 program (Stuiver et al., 1998). The new age determinations (Table 1), as well as a previously determined age for the large H2 eruption of the Hudson volcano (Naranjo and Stern, 1998), were used to control the chronology of the tephra in the LLT (Fig. 6) and other cores (Fig. 3; Table 5). The average age of the undated tephra in the LLT core and the other cores from near Coyhaique (Tables 5 and S2 of the

Figure 5. (color online) Photographs and photomicrographs of the three geochemically distinct tephra derived from the different source volcanoes. The source volcanoes of these tephra are determined by both the geochemical characteristics of these tephra (Fig. 4) and isopach maps. Abbreviations are for glass (gls), plagioclase (plg), orthopyroxene (opx), clinopyroxene (cpx), olivine (olv), amphibole (amph). **A, B, and C**. Hudson-derived H2 tephra which is light brown in color with tan pumice and a minor proportion of dark mafic components and containing phenocryst of plagioclase, orthopyroxene and minor clinopyroxene and olivine, and tan volcanic glass with no mineral microlites and highly deformed cylindrical vesicles. This tephra occurs in all the cores in the region but is thickest just to the east of Hudson volcano. **D, E, and F.** Mentolat-derived Q3 eruption which is light grey in color with small clasts of white rhyolitic pumice and small proportion of dark mafic components. The Q3 tephra contains abundant phenocrysts of plagioclase, orthopyroxene, amphibole, and a smaller proportion of clinopyroxene and olivine. Tephra glass from the Mentolat-derived tephra are colorless with circular vesicles and no mineral microlites. This tephra is chemically, texturally and mineralogically identical to Mentolat-derived tephra G and H in cores from the Río Cisnes valley just east of this volcano (Weller et al., 2017). **G, H, I.** Macá-derived MAC1 eruption (Naranjo and Stern, 2004) which is geochemically and petrographically similar to other LA-type tephra that may be sourced from either Macá, Cay or one of the monogenetic centers (MEC) from the region. The MAC1 eruption and other LA geochemical tephra are generally dark brown to black in color with black scoria and abundant phenocrysts of plagioclase, olivine, and clinopyroxene and either lacking or containing a small proportion of orthopyroxene and amphibole. Tephra glass from these eruptions is generally dark brown with circular vesicles and varying proportions of mineral microlites or black volcanic glass.

supplementary material) were estimated with the OxCal program using the Southern Hemisphere radiocarbon calibration data (Hogg et al., 2013). The OxCal program uses a Bayesian method, which incorporates information on both the depth and ordering of the tephra deposits and the available radiocarbon ages (Bronk Ramsey, 2008). This information was used to determine a representative set of possible ages for each tephra in the sedimentary record (Fig. 6; Bronk Ramsey, 2008). For this analysis, the P sequence mode was applied with a k parameter (Table S3 and file SM1 of the supplementary material) calculated with the method outlined in Bronk Ramsey (2008) using three distinct horizons observed in every lake core; the H2 eruption of Hudson, the Q3 eruption of Mentolat and the base of the Hudson derived sequence of 10 closely spaced eruptions (S1-S10; Figs. 2, 3 and 6). For these calculations, tephra layers greater than 1 cm in thickness were all subtracted from the total integrated thickness of each core.

RESULTS

General

The results include a lithostratigraphic description (Table S1 of the supplementary material) and bulk tephra trace element

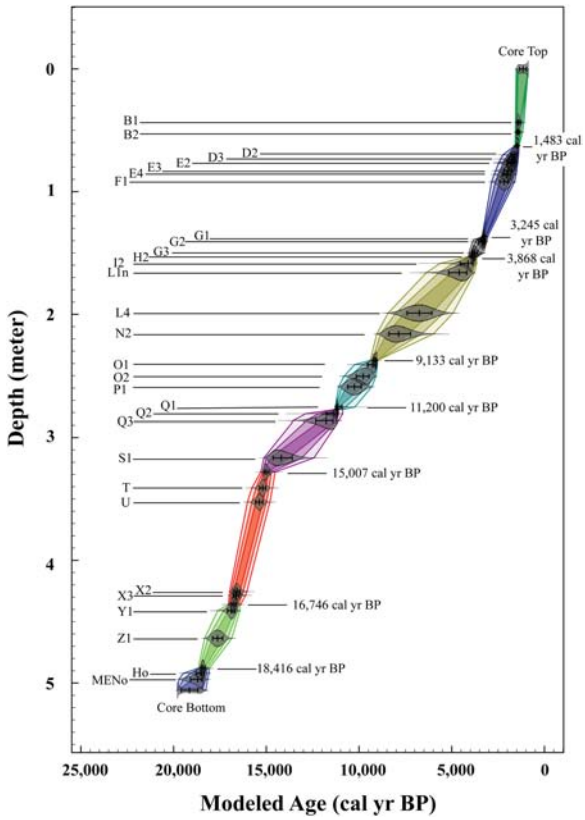

Figure 6. (color online) Age versus depth model for the tephra in the Laguna La Trapananda sediment core, calculated using OxCal 4.2 (Bronk Ramsey, 2008) with the Southern Hemisphere radiocarbon calibration data SHCal13 (Hogg et al., 2013). The seven ages from the LLT core (Table 1) and for the Hudson H2 eruption (Naranjo and Stern, 1998, 2004) that control the model are indicated on the right of the curve, and the ages of all the tephra are tabulated in Table S3 of the supplementary material.

contents (Table 2, 3 and 4) of the 19 tephra sampled, the correlation of the tephra observed in the LLT core (Fig. 2) with those in other lake cores from the region (Figs. 3 and S1-S8 of the supplementary material), source volcano identification, as well as the modeled average age for 56 tephra observed in both the LLT core and some or all of the other cores from near Coyhaique (Table 5).

Tephra correlations

Correlation of the tephra between the cores (Fig. 3) is based on three criteria: 1) first and most significantly the stratigraphic relationship between the cores; 2) second the tephra lithostratigraphic characteristics such as glass color and morphology, vesicle abundance and morphology, the presence of mineral microlite, and the identity and abundance of mineral phenocrysts (Fig. 5; Table S1 of the supplementary material), and 3) bulk tephra trace element chemistries as compared against published trace element contents of lavas and tephra from the volcanoes of the SSVZ (Fig. 4, Table 2, 3 and 4). Samples that were not collected from the LLT core but were collected from the other lacustrine sediment cores from near Coyhaque were correlated amongst each other based on their similar stratigraphic relation. The tephra are sourced to specific volcanoes based on the fact that isopach maps of some widely distributed tephra deposits such as Ho and H2 derived from the Hudson volcano (Weller et al., 2014), MAC1 derived from Macá (Naranjo and Stern, 2004) and thick tephra deposits in the Río Cisnes valley clearly derived from Mentolat (Weller et al., 2017), all have the same distinctive mineralogical, textural and geochemical characteristics described in detail above (Figs. 4 and 5).

Among the 19 tephra layers sampled from Laguna Las Trapananda, seven eruptions are therefore attributed to small to medium sized eruptions of Mentolat (B2, I2, L1n, L4, Q3, T and MENo; Fig. 2), two of which (I2 and L4) were not previously recognized in the other lake cores from 15-57 km to the south near Coyhaique. Six eruptions are attributed to explosive eruptions of Hudson volcano (E2, H2, S3, U1, Z1 and Ho; Fig. 2), one of which (U1) was observed in the lake cores near Coyhaique, but was not previously sampled. One tephra (D3; Fig. 2) is attributed to a medium sized explosive eruption of Macá, and source volcanoes for five other tephra (E3, N2, O2, P1 and Y1; Fig. 2) may be either Macá, Cay, or one of the MEC.

Mentolat Tephra

Of the seven sampled tephra attributed to eruptions of Mentolat (Fig. 2), five (B2, L1n, Q3 (previously MEN1), T and MENo) correspond to tephra observed in other lake cores near Coyhaique (Weller et al., 2015, 2014). All of these tephra contain clear colorless volcanic glass with rounded vesicles, but lacking mineral microlites, and have abundant phenocrysts of plagioclase, orthopyroxene, amphibole, and minor clinopyroxene and olivine (Fig. 5). All of these tephra are light grey in color containing either fine or coarse white rhyolitic pumice clasts and variable proportions of dark grey to black mafic components. These tephra are all VLA geochemical type (Fig. 4; Table 3) which generally fall within the fields defined by previously reported analyses of Mentolat derived tephra and lavas.

Two other sampled tephra (I2 and L4) are both VLA petrochemical type deposits (Fig. 4; Table 3) and also contain tephra glass and mineral characteristics similar to Mentolat derived tephra (Table S1 of the supplementary material). One deposit, tephra I2, is similar to a previously uncorrelated deposit from Lago Tranquilo (Weller et al., 2015). The other tephra (L4) is not observed in the other lake cores from the region but has trace element (Fig. 4; Table 3) and petrographic characteristics (Table S1 of the supplementary material) similar to other Mentolat derived tephras and we source this eruption from Mentolat. It underlies two distinctive sequences of three tephra each called L2a-c and L3a-c, but these have not been sampled.

Most significantly, the new age determinations indicate that the Mentolat-derived tephra previously identified as

Table 2. Trace element concentrations (ppm) of the Hudson derived tephra form LLT and other cores from near Coyhaique.

Lake	LLT	Avg*	LLT	Avg*	LLT	Avg*	LLT	LLT	Avg*	LLT	Avg*
Section	T2	-	T3	-	T5	-	T5	T6	-	T7	-
Depth	52-55	-	40-45	-	24-25	-	57	79-81	-	20-40	-
Chemical Type	HA	HA	HA	HA	HA	HA	HA	LA		HA	HA
Source	Hudson	Hudson	Hudson	HUD	Hudson	Hudson	Hudson	Hudson	Hudson	Hudson	Hudson
Tephra	E2	E2	H2	H2	S3	S3	U	Z1	Z1	Ho	Ho
Lab No.	DW15-03	-	DW15-06	-	DW15-15	-	DW15-17	DW15-19	-	DW15-20	-
n	1	7	1	10	1	4	1	1	16	1	22
Ti	8538	7867	6767	7221	11785	10406	13387	9318	9846	7998	8350
V	302	256	184	146	344	261	369	340	306	232	208
Cr	46	51	17	13	24	18	19	53	35	DL	18
Mn	1191	1173	1066	1147	1210	1326	1239	1165	1179	1119	1134
Co	41	41	40	20	38	35	79	34	38	41	33
Ni	55	48	38	26	52	30	48	59	29	39	25
Cu	52	78	17	55	48	93	49	43	108	33	231
Zn	139	112	132	110	162	121	155	132	108	147	108
Rb	33	28	61	54	25	23	33	33	30	56	41
Sr	598	528	392	368	660	540	554	562	478	402	451
Y	29	24	38	37	34	35	35	28	29	35	31
Zr	226	195	364	349	270	256	227	165	183	296	226
Nb	14	10	19	17	14	13	11	8	9	19	13
Cs	1.0	0.4	1.6	1.3	0.9	0.5	1.1	2.1	0.8	2.8	1.1
Ba	453	390	702	688	504	511	469	408	386	617	514
La	28.6	25.1	39.3	38.7	35.1	34.0	28.6	22.6	23.6	34.5	28.6
Ce	65.7	55.9	88.7	84.7	81.7	78.7	68.9	52.5	53.8	77.5	63.4
Pr	8.09	6.9	10.47	10.22	10.34	10.1	8.84	6.63	6.9	9.3	7.94
Nd	32.8	29.3	41.2	41.1	44.3	42.2	38.4	28.1	29.4	38.4	33.1
Sm	7.44	6.05	9.81	8.59	9.49	8.77	9.09	6.77	6.51	9.36	7.19
Eu	2.68	1.75	3.33	2.49	3.22	2.56	3.06	2.42	2.07	3.02	2.17
Gd	10.54	6.9	13.19	9.97	13.35	9.7	12.42	9.09	7.6	12.2	8.23
Tb	1.18	0.80	1.42	1.20	1.31	1.24	1.34	1.01	0.98	1.33	1.04
Dy	5.54	4.73	7.09	6.93	6.97	6.64	7.25	5.31	5.49	6.74	5.82
Ho	1.08	0.86	1.26	1.32	1.21	1.27	1.24	0.95	1.07	1.24	1.12
Er	3.24	2.78	4.39	4.27	4.01	3.89	3.93	3.15	3.29	4.25	3.43
Tm	0.39	0.30	0.51	0.50	0.36	0.47	0.40	0.28	0.41	0.47	0.41
Yb	2.76	2.46	3.85	3.95	3.09	3.35	3.23	2.74	2.88	3.45	3.09
Lu	0.38	0.26	0.52	0.55	0.40	0.37	0.37	0.28	0.40	0.46	0.39
Hf	5.0	4.9	7.7	8.0	5.3	5.7	4.6	3.7	4.4	9.1	5.6
Pb	6.9	6.9	10.7	11.2	6.6	6.4	6.7	6.4	5.6	11.3	8.5
Th	1.9	4.1	3.3	6.0	1.6	3.8	1.7	2.0	4.0	3.0	5.3
U	0.9	0.8	1.5	1.4	0.8	0.6	0.9	1.0	0.8	1.5	1.2

*Average or single tephra trace element contents from Weller et al. (2015).

Table 3. Trace element concentrations (ppm) of the Mentolat derived tephra form LLT and other cores from near Coyhaique.

Lake	LLT	Avg*	LLT	LTr*	LLT	Avg*	LLT	LLT	Avg*	LLT	Avg*	LLT	Avg*
Section	T2	-	T3	AT5	T3	-	T3	T4	-	T5	-	T7	-
Depth	17-25	-	49-49.5	49	56-56.5	-	89-89.5	79-82.5	-	46	-	44-46	-
Chemical Type	VLA	VLA	VLA	VLA	VLA	VLA	VLA	VLA	VLA	VLA	VLA	VLA	VLA
Source	Mentolat	Mentolat	Mentolat	Mentolat	Mentolat	Mentolat	Mentolat	Mentolat	Mentolat	Mentolat	Mentolat	Mentolat	Mentolat
Tephra	B2	B2	I2	I2	L1n	L1n	L4	Q3	Q3	T	T	MENo	MENo
Lab No.	DW15-01	-	DW15-07	CS 4112	DW15-08	-	DW15-09	DW15-13	-	DW15-16	-	DW15-21	-
n	1	4	1	1	1	2	1	1	7	1	8	1	7
Ti	5937	7069	6456	6560	6639	7137	5566	3448	4761	5920	6228	4945	4728
V	279	299	320	360	215	270	269	184	185	211	161	281	208
Cr	14	18	21	16	24	17	24	DL	22	25	14	24	21
Mn	1478	1452	1210	1581	1032	1164	1325	1127	1607	1043	1104	1148	1030
Co	39	34	57	45	72	31	115	26	34	80	47	35	30
Ni	36	32	45	37	50	35	47	50	30	50	20	51	24
Cu	32	71	43	73	31	71	44	16	22	33	137	22	69
Zn	137	133	142	129	134	131	138	101	117	121	118	109	87
Rb	11	15	23	14	38	30	23	14	7	33	29	11	23
Sr	529	442	478	442	488	505	513	616	556	497	377	517	411
Y	19	20	23	18	28	24	21	16	12	23	26	14	16
Zr	76	87	123	107	166	133	109	83	49	104	128	55	73
Nb	27	4	5	3	7	4	5	3	2	4	5	2	3
Cs	0.9	0.7	1.9	0.5	1.4	0.7	2.6	0.9	0.2	4.0	1.3	0.9	1.4
Ba	155	186	254	173	452	355	240	184	113	322	310	134	206
La	7.0	8.3	13.1	8.5	22.3	16.6	13.8	8.0	5.5	13.1	13.7	5.4	8.4
Ce	16.9	19.9	31.0	20.7	50.9	38.9	31.8	19.2	13.7	30.6	32.6	13.4	19.1
Pr	2.3	2.67	3.9	2.7	6.42	5.0	4.30	2.59	1.9	3.85	4.3	1.73	2.5
Nd	11.1	13.3	17.5	13.7	27.1	22.9	18.9	12.1	9.0	17.3	19.4	8.5	11.2
Sm	3.06	3.47	4.39	3.17	6.56	5.17	4.46	3.08	2.16	4.64	4.97	2.41	2.83
Eu	1.34	1.09	1.62	0.84	2.24	1.42	1.60	1.28	0.88	1.79	1.55	0.91	0.98
Gd	4.1	4.17	6.0	4.3	8.68	6.2	5.97	3.92	2.7	6.04	5.9	3.25	3.4
Tb	0.59	0.54	0.70	0.46	0.97	0.69	0.65	0.44	0.31	0.69	0.80	0.33	0.38
Dy	3.10	3.41	4.17	3.38	5.07	4.61	3.72	2.66	2.21	3.95	4.81	2.42	2.77
Ho	0.65	0.62	0.78	0.56	1.00	0.81	0.71	0.43	0.35	0.76	0.94	0.41	0.54
Er	1.94	2.20	2.55	2.04	3.08	2.76	2.30	1.72	1.32	2.53	2.96	1.46	1.79
Tm	0.25	0.20	0.26	0.20	0.34	0.28	0.23	0.11	0.14	0.25	0.35	0.09	0.19
Yb	1.82	1.99	2.23	2.01	2.76	2.46	2.03	1.56	1.25	2.32	2.74	1.27	1.65
Lu	0.27	0.21	0.28	0.20	0.32	0.27	0.22	0.14	0.09	0.24	0.33	0.11	0.20
Hf	3.5	2.7	2.8	2.5	3.8	3.0	2.5	2.0	1.4	2.6	3.7	1.4	2.2
Pb	4.0	5.3	6.2	4.0	9.1	6.9	6.4	4.8	3.2	8.9	9.6	3.9	6.2
Th	0.4	1.9	1.0	0.8	1.7	2.1	1.0	0.5	0.6	1.9	3.2	0.4	2.2
U	0.3	0.3	0.6	0.3	1.1	0.7	0.7	0.4	0.1	1.1	0.9	0.3	0.8

*Average or single tephra trace element contents from Weller et al. (2015).

Table 4. Trace element concentrations (ppm) of the Macá, Cay, or MEC derived tephra form LLT and other cores from near Coyhaique.

Lake	LLT	Avg*	LLT	Avg*	LLT	LU*	LLT	Avg*	LLT	Avg*	LLT	Avg*
Section	T2	-	T2	-	T4	ET6	T4	-	T4	-	T6	-
Depth	46-49	-	58.5-59	-	7-8	53	40-43	-	51-53	-	58	-
Chemical Type	LA	LA	LA	LA	LA	LA	LA	LA	LA	LA	LA	LA
Source	Macá	Macá	M/C/MEC	M/C/MEC	M/C/MEC	M/C/MEC	M/C/MEC	M/C/MEC	M/C/MEC	M/C/MEC	M/C/MEC	M/C/MEC
Tephra	MAC1/D3	MAC1/D3	E3	E3	N2	N2	O2	O2	P1	P1	Y1	Y1
Lab No.	DW15-02	-	DW15-04	CS 4106	DW15-10	CS 4133	DW15-11	-	DW15-12	-	DW15-18	-
n	1	7	1	1	1	1	1	5	1	8	1	5
Ti	5481	6820	7931	6888	7048	6617	6861	6230	6208	6524	7127	6740
V	236	222	394	386	270	292	244	204	218	213	265	261
Cr	120	102	55	38	19	38	17	18	19	22	24	18
Mn	944	1110	1290	1395	1199	1065	1226	1078	1052	1122	1278	1153
Co	56	45	155	45	53	30	27	29	33	34	62	35
Ni	101	84	58	39	51	40	50	32	50	35	48	21
Cu	35	92	74	127	37	140	31	69	19	91	33	125
Zn	104	98	142	135	145	103	143	107	124	115	149	110
Rb	16	19	18	16	24	37	22	17	23	16	27	21
Sr	688	580	522	419	516	477	496	452	552	452	535	470
Y	18	20	24	16	25	23	25	21	23	20	26	23
Zr	120	157	91	83	109	142	98	86	109	78	113	99
Nb	12	7	7	3	9	3	4	4	4	4	4	4
Cs	0.6	0.2	1.4	0.8	1.4	1.0	1.4	0.5	1.0	0.5	2.4	1.0
Ba	245	308	214	156	273	351	274	229	293	224	301	259
La	14.9	19.5	10.4	6.4	12.4	15.5	11.4	9.6	13.4	9.5	14.3	12.8
Ce	35.1	44.8	25.8	17.3	29.5	35.3	26.7	22.9	31.6	22.8	34.0	29.4
Pr	4.53	5.6	3.56	2.2	3.83	4.61	3.72	3.1	4.07	3.1	4.42	3.9
Nd	19.4	23.9	16.2	11.7	18.1	20.0	17.5	14.5	18.5	14.0	20.3	17.4
Sm	4.37	5.00	4.32	2.76	4.93	4.62	4.84	3.73	4.87	3.69	5.06	4.29
Eu	1.61	1.50	1.67	0.87	1.79	1.15	1.79	1.17	1.84	1.23	1.78	1.39
Gd	6.05	5.8	5.93	3.7	6.62	5.45	6.19	4.5	6.55	4.4	7.04	5.1
Tb	0.69	0.65	0.82	0.39	0.79	0.62	0.76	0.56	0.73	0.57	0.81	0.70
Dy	3.35	3.98	4.26	3.03	4.35	4.10	4.51	3.71	4.34	3.71	4.73	4.12
Ho	0.63	0.72	0.85	0.54	0.84	0.76	0.81	0.67	0.80	0.74	0.83	0.83
Er	1.99	2.28	2.46	1.78	2.70	2.56	2.66	2.28	2.53	2.22	2.89	2.52
Tm	0.22	0.22	0.29	0.18	0.28	0.27	0.26	0.21	0.24	0.28	0.27	0.30
Yb	1.71	2.03	2.22	1.61	2.44	2.38	2.42	1.99	2.22	2.11	2.56	2.26
Lu	0.21	0.17	0.31	0.17	0.26	0.31	0.28	0.14	0.25	0.24	0.31	0.29
Hf	3.0	3.7	2.4	2.2	6.2	3.3	2.6	2.4	2.5	2.6	2.7	2.8
Pb	3.5	5.3	5.9	5.0	7.5	7.6	7.3	6.7	6.0	6.8	8.4	7.3
Th	0.8	2.5	0.7	1.1	0.9	2.7	0.8	1.4	1.1	1.9	1.6	2.9
U	0.4	0.5	0.6	0.4	0.7	0.8	0.6	0.5	0.6	0.4	0.9	0.7

*Average or single tephra trace element contents from Weller et al. (2015).

Table 5. Average modeled age for tephra observed in the lake cores near Coyhaique.

Tephra	Source	Age (cal yr BP)	1σ	Tephra	Source	Age (cal yr BP)	1σ
A1	M/C/MEC	793	2590	**N**	Hudson	8233	1354
A2	-	1021	2063	**N2**	M/C/MEC	8864	524
B1	-	1340	1505	**O1**	Mentolat	9261	675
B2	Mentolat	1426	1300	**O2**	M/C/MEC	9417	880
C1	Hudson	1532	312	**P1**	M/C/MEC	10613	1126
C2	Hudson	1612	421	**P2**	Hudson	10724	1071
D1	Mentolat	1774	498	**Q1**	Mentolat	11142	778
D2	Hudson	1872	544	**Q2**	Mentolat	11378	623
D3	Macá	1922	577	**Q3**	Mentolat	11407	948
E1	Hudson	1900	690	**S1**	Hudson	14647	1114
E2	Hudson	1965	600	**S10**	Hudson	14967	172
E3	M/C/MEC	1956	520	**T**	Mentolat	15120	548
E4	-	2058	747	**U1**	Hudson	15473	1189
F1	Hudson	2211	788	**U2**	-	15487	1135
F2	Hudson	2235	675	**U3**	-	15750	668
F3	Hudson	2494	756	**V**	Hudson	15956	1572
G1	M/C/MEC	3314	491	**Wn**	M/C/MEC	16437	557
G2	M/C/MEC	3614	600	**Ws**	Hudson	16210	1642
G3	M/C/MEC	3771	519	**X1**	Hudson	16608	479
H2	Hudson	3868	236	**X2**	Hudson	16654	577
I1	Hudson	4528	1059	**X3**	Hudson	16695	538
I2	Mentolat	4793	918	**Y1**	M/C/MEC	16878	640
J	Hudson	5337	1394	**Y2**	-	17467	624
L1n	Mentolat	5372	1416	**Z1**	Hudson	17575	831
K	Hudson	5434	1152	**Ho**	Hudson	18459	497
L1s	M/C/MEC	6450	865	**Z3**	M/C/MEC	18497	712
L4	Mentolat	6747	665	**MENo**	Mentolat	18672	733
M	Hudson	8139	1261	**Z5**	M/C/MEC	18844	876

M/C/MEC- Macá, Cay or Monogenetic eruptive center (MEC).

MEN1 in the other cores from near Coyhaique (Weller et al., 2015, 2014) is older than the MEN1 tephra deposit described in outcrop by Naranjo and Stern (2004) and in lake cores further south by Stern et al. (2016) and McCulloch et al. (2016), and its name has been changed accordingly to Q3 (Figs. 2 and 3).

Hudson Tephra

Six tephra deposits (E2, H2, S3, U1, Z1 and Ho) from LLT are attributed to explosive eruptions from Hudson (Fig. 2). These tephras include the ~3,900 cal yr BP H2 eruption (Naranjo and Stern, 1998), the large late-glacial Ho eruption previously dated at ~17,400 cal yr BP from lake cores near Coyhaique (Weller et al., 2015, 2014), and several smaller eruptions including tephra S3 of the sequence of 10 (S1-S10) closely spaced Hudson-derived eruptions dated at approximately ≤15,000 cal yr BP. Tephra U of the LLT lake core corresponds to the youngest of the three tephra U1-U3 from near Coyhaique, which were not previously sampled.

These tephra are all HA geochemical type deposits (Fig. 4; Table 2), and are all generally similar in appearance and color to other Hudson derived tephra, including the H2 tephra, which contains a mixture of both light brown to tan pumice clasts and less abundant dark mafic material. These deposits consist of either tan volcanic glass with no mineral microlites and abundant elongated vesicles or dark brown glass with few circular vesicles and variable amounts of mineral microlites (Fig. 5). Commonly observed phenocrysts include plagioclase, clinopyroxene, orthopyroxene, and minor olivine, but not amphibole.

Macá, Cay, and Minor Eruptive Centers (MEC) Tephra

Tephra D3 (Fig. 2), which is attributed to the small to medium sized explosive MAC1 eruption of Macá (Naranjo and Stern, 2004; Weller et al., 2015), is also observed in the LLT core. Five additional LA geochemical type tephra (Fig. 4) could be sourced from either Macá, Cay, or one of the MEC (Fig. 2). Four of these tephra (E3, O2, P1, and Y1; Weller et al., 2015) correspond to previously described eruptions. One tephra, N2, occurs in the same stratigraphic position and has similar LA-type geochemistry to a previously uncorrelated tephra from Lake Unco (Fig. 3). All of the LA geochemical type eruptions consist of dark brown and/or black glass which contains variable amounts of mineral microlites and circular vesicles. Common phenocrysts include olivine,

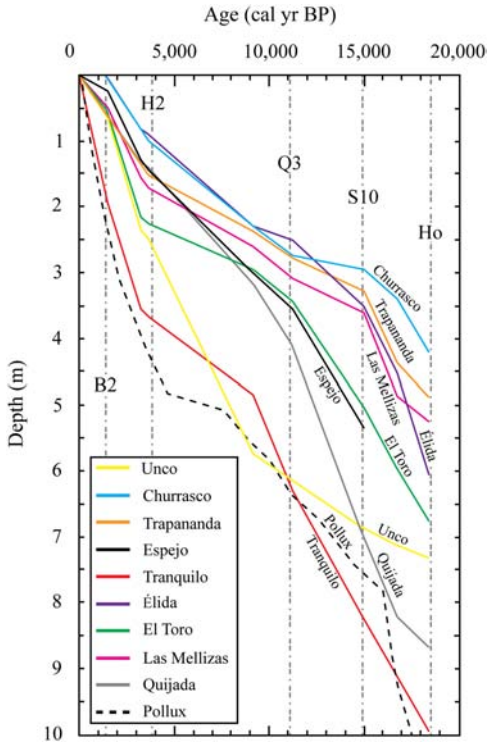

Figure 7. (color online) Sedimentation profiles for Laguna La Trapananda and the other eight lake cores from near Coyhaique (Weller et al., 2015), from the surface to the base of each core, using the new radiocarbon age estimates (Tables 1 and S2 of the supplementary material). The figure includes one previously published profile, based on an independent sets of internal age ages, from Mallín el Pollux (Markgraf et al., 2007). Tephra with a thickness of 1 cm or greater have been subtracted from the total integrated length of the sediments in the cores.

clinopyroxene, and plagioclase with less common orthopyroxene, and in a few cases a small amount of amphibole (Fig. 5).

Tephra Ages

The new radiocarbon age dates are reported in Table 1. The deepest radiocarbon age in the LLT core (18,416 ± 98 cal yr BP; Fig. 2), which was sampled directly above the late-glacial Ho eruption of Hudson, is similar to the ages of Ho determined in a core from Lago Castor (Fig. 1) 28 km to the south of LLT (17,500-18,410 cal yr BP; Van Daele et al., 2016) and estimated in a core from ~110 km north in the Río Cisnes valley (18,820 yr BP; Stern et al., 2015), but ~1000 years older than the previous determination of the age of this tephra in other cores from near Coyhaique (17,370 ± 70 cal yr BP; Miranda et al., 2013; Weller et al., 2014). The new age (15,007 ± 128 cal yr BP; Table 5) determined just below the S1-S10 sequence of tephra (at 34 cm depth in section T5; Fig. 2) is similar to the age (14,932 cal yr BP; Weller et al., 2015) previously estimated for the beginning of this sequence of tephra.

The age estimates from the Bayesian modeling of the 56 tephra found in the LLT core and in each of the eight other lake cores from near Coyhaique are reported in Table S2 of the supplementary material, and the average age of each of these 56 tephra found in some or all the lake sediment cores from near Coyhaique are reported in Table 5. In a few instances, the average model age of stratigraphically older tephra are calculated to have younger ages than the overlying tephra deposit. This is the result of some tephra being observed in all the lake cores, while other tephra are only preserved in a few lakes and their age estimate is biased towards the modelled ages from these lakes. However, the average age estimates for these tephra are all within the error estimates of the stratigraphically associated tephra (Table 5).

DISCUSSION

The 19 sampled tephra from the Laguna La Trapananda sediment core are similar petrologically, geochemically, and share similar stratigraphic relations, with the tephra observed in other lake cores 15-57 km to the south (Fig. 1; Weller et al., 2015), which allows for their correlation with the tephra in these other cores (Figs. 3 and S1-S8 of the supplementary material). Based on these correlations, the new radiocarbon age determinations are also correlated amongst 56 tephra observed in the other lake sediment cores taken from the region (Table 5; Weller et al., 2015). This provides the most detailed tephrochronology available for any sector of the Andean arc, most parts of which are constrained only by subaerial tephra exposure reflecting just the largest eruptions (Fontijn et al., 2016, 2014).

The ages confirm that Mentolat, Hudson, Macá and possibly Cay or one of the MEC have produced regionally widespread tephra since the late Pleistocene deglaciation of the region (Bendle et al., 2017; Miranda et al., 2013) and throughout the Holocene. Among the 56 tephra chronologically constrained since 18,850 cal yr BP (on average, one event every 340 yrs), 25 were produced by explosive eruptions of Hudson (on average, one event every 740 yrs), 14 by explosive eruptions of either Macá, Cay, or one of the MEC (on average, one event every 1,350 yrs), 11 by Mentolat (on average, one event every 1,710 yrs), and 6 have not been sampled or sourced. Hudson volcano, located just east of the Chile Rise-Trench triple junction, has been the most active in terms of both volume (Völker et al., 2011; Weller et al., 2015, 2014) and frequency (Table 5) of explosive eruptions, and both average recurrence rates and eruptive volumes have decreased northwards away from the Chile Rise-Trench triple junction.

The ages also suggest that eruption rates of the individual volcanoes in the southernmost SSVZ were essentially uniform since late-glacial times, with no clear post-glacial increase in volcanic activity as has been suggested for further north in the SVZ by Watt et al. (2013), Fontijn et al. (2016, 2014) and Rawson et al. (2016). However, occasional episodic concentrations of activity from a single volcano in

~200 to 400 year periods do occur, producing for instance the S1 to S10 sequence of Hudson eruptions, the Q1 to Q3 sequence of Mentolat eruptions, and the G1 to G3 sequence of eruptions of Macá, Cay or a MEC center.

Concerning specific tephra, the modelled age for tephra D3 (1,922 ± 215 cal yr BP; Table 5), which Weller et al. (2015) attributed to the late Holocene MAC1 eruption of Macá, is similar to the radiocarbon age date of tephra T3 (1,860 ± 30 cal yr BP; Elbert et al., 2013) from Lago Castor (Fig. 1), but older than the age estimate obtained from a proximal subaerial soil exposure of this tephra (1,440 ± 60 cal yr BP; Naranjo and Stern, 2004). The new radiocarbon age determinations also indicate that the tephra previously correlated with the MEN1 eruption of Mentolat from the eight other lake cores near Coyhaique (Weller et al., 2015) is too old to correspond to the 7,690 ± 60 cal yr BP outcrop deposit described by Naranjo and Stern (2004) and the distal MEN1 tephra deposit observed further south in lake cores near the town of Cochrane (McCulloch et al., 2017; Stern et al., 2016). This tephra, now named Q3, represents an older early-Holocene eruption of Mentolat volcano.

The area of the southernmost SSVZ is of particular interest to paleoclimatologists due to its preservation of late-glacial to recent climate change records at mid-latitudes of the Southern Hemisphere (de Porras et al., 2014, 2012; Elbert et al., 2013; Markgraf et al., 2007; McCulloch et al., 2017; Miranda et al., 2013; Moreno et al., 2010; Van Daele et al., 2016). Sedimentation rates in the cored lakes may be a possible proxy for climate change to the extent that they reflect changes in precipitation rate and vegetation cover. Based on the age estimates presented in Table 5, depth versus age sedimentation profiles were generated for the LLT core (Fig. 6) and for other lake sediment cores from the Coyhaique area (Fig. 7; Weller et al., 2015). The sedimentation profiles, constrained by our tephra age estimates, indicate that in each lake there have been intervals of relatively rapid and slower sediment accumulation. However, the timing of the changes in sedimentation rate clearly varies amongst the lakes. For example, many of the lakes, including LLT (at 1,160 m the highest lake cored), Churrasco (798 m), Lago Pollux (725 m), Las Mellizas (751 m) and Ėlida (570 m), experienced relatively rapid accumulation of material after deglaciation until approximately 15,000 cal yr BP, after which sedimentation rates in these lakes decreased (Fig. 7). On the other hand, decreasing rates of sediment accumulation takes place much later, at approximately 10,000 cal yr BP or after (Fig. 7), for several other lakes such as Tranquilo (953 m), Quijada (723 m), El Toro (675 m) and Espejo (at 310 m the lowest elevation lake cored). This indicates that between the late-glacial and early Holocene each lake has its own complex sedimentation history, and that the uniformity in the timing of the sedimentation rate changes previously suggested by Weller et al. (2015) is absent. These changes were not influenced by lake elevation, and the temporal differences in when these changes in sediment rates occurred in each lake suggests that they are unlikely to reflect regional climate change.

The early Holocene decrease in the sediment accumulation rate is followed by a more rapid sedimentation rate starting in all the cores after the H2 eruption at approximately 3,900 cal yr BP (Fig. 7). This rapid change in the sedimentation profiles is also observed in Mallín el Pollux (Markgraf et al., 2007) with an independent chronology, suggesting that this mid-Holocene change was regional, potentially reflecting a change from local variables influencing the sedimentation rates in each basin towards more regional controls, possibly as a result of increasing westerly-driven precipitation associated with both an expanded and strengthened southern westerly wind belt (SWWB; Van Daele et al., 2016) that effected all the small lacustrine systems located in southern Chile.

CONCLUSIONS

New radiocarbon ages within a lake sediment core from the Laguna La Trapananda in southern Chile allow for the estimation of the ages of 56 tephra (Table 5) observed in this and other lake cores from the region. These age estimates provide a tool for evaluating eruption rates in this region, which are found to be essentially uniform since late-glacial time. The new age estimates also allow the determination of sedimentation rates in a number of lakes which have been cored for paleoclimate and paleoecologic studies in this region of central Patagonia, and these rates are found to be both variable through time and different amongst each lake. Further applications and refinements of this tephrochronology tool is expected in the future, as this region is of special interest to volcanologists, due to its proximity to the Chile Rise-Trench triple junction, as well as to paleoclimatologists, due to its preservation of late-glacial to recent climate change records at mid-latitudes of the Southern Hemisphere.

ACKNOWLEDGMENTS

We thank two anonymous reviewers for their constructive comments which greatly enhanced the quality of this manuscript and the Reserva Nacional La Trapananda (CONAF) for permission to core the Laguna La Trapananda, and the Hospital Público San Juan de Dios de La Serena for the digital X-ray images of the core. This work was funded by FONDECYT (Chile) grant #1130128.

SUPPLEMENTARY MATERIAL

To view supplementary material for this article, please visit https://doi.org/10.1017/qua.2018.81

REFERENCES

Alloway, B.V., Moreno, P.I., Pearce, N.J.G., De Pol-Holz, R., Henríquez, W.I., Pesce, O.H., Sagredo, E., Villarosa, G., Outes, V., 2017a. Stratigraphy, age and correlation of Lepué Tephra: a widespread c. 11 000 cal a BP marker horizon sourced from the Chaitén Sector of southern Chile. *Journal of Quaternary Science*. 32, 795–829. https://doi.org/10.1002/jqs.2976

Alloway, B.V., Pearce, N.J.G., Moreno, P.I., Villarosa, G., Jara, I., De Pol-Holz, R., Outes, V., 2017b. An 18,000 year-long eruptive record from Volcán Chaitén, northwestern Patagonia: Paleoenvironmental and hazard-assessment implications. *Quaternary Science Reviews*. 168, 151–181. https://doi.org/10.1016/j.quascirev.2017.05.011

Bendle, J.M., Palmer, A.P., Thorndycraft, V.R., Matthews, I.P., 2017. High-resolution chronology for deglaciation of the Patagonian Ice Sheet at Lago Buenos Aires (46.5°S) revealed through varve chronology and Bayesian age modelling. *Quat. Sci. Rev*. 177, 314–339. https://doi.org/10.1016/j.quascirev.2017.10.013

Bertrand, S., Castiaux, J., Juvigné, E., 2008. Tephrostratigraphy of the late glacial and Holocene sediments of Puyehue Lake (Southern Volcanic Zone, Chile, 40°S). *Quaternary Research*. 70, 343–357. https://doi.org/10.1016/j.yqres.2008.06.001

Bronk Ramsey, C., 2008. Deposition models for chronological records. *Quaternary Science Reviews*. 27, 42–60. https://doi.org/10.1016/j.quascirev.2007.01.019

Carel, M., Siani, G., Delpech, G., 2011. Tephrostratigraphy of a deep-sea sediment sequence off the south Chilean margin: New insight into the Hudson volcanic activity since the last glacial period. *Journal of Volcanology and Geothermal Research*. 208, 99–111. https://doi.org/10.1016/j.jvolgeores.2011.09.011

D'Orazio, M., Innocenti, F., Manetti, P., Tamponi, M., Tonarini, S., González-Ferrán, O., Lahsen, A., Omarini, R., 2003. The Quaternary calc-alkaline volcanism of the Patagonian Andes close to the Chile triple junction: Geochemistry and petrogenesis of volcanic rocks from the Cay and Maca volcanoes (~45°S, Chile). *Journal of South American Earth Sciences*. 16, 219–242. https://doi.org/10.1016/S0895-9811(03)00063-4

Daga, R., Guevara, S.R., Arribére, M., 2016. Journal of South American Earth Sciences New records of late Holocene tephras from Lake Futalaufquen (42.8°S), northern Patagonia. *Journal of South Amerian Earth Sceince* 66, 232–247. https://doi.org/10.1016/j.jsames.2015.12.003

de Porras, M.E., Maldonado, A., Abarzúa, A.M., Cárdenas, M.L., Francois, J.P., Martel-Cea, A., Stern, C.R., Méndez, C., Reyes, O., 2012. Postglacial vegetation, fire and climate dynamics at Central Chilean Patagonia (Lake Shaman, 44°S). *Quaternary Science Reviews*. 50, 71–85. https://doi.org/10.1016/j.quascirev.2012.06.015

de Porras, M.E., Maldonado, A., Quintana, F.A., Martel-Cea, A., Reyes, O., Méndez, C., 2014. Environmental and climatic changes in central Chilean Patagonia since the Late Glacial (Mallín El Embudo, 44° S). *Climate of the Past* 10, 1063–1078. https://doi.org/10.5194/cp-10-1063-2014

Elbert, J., Wartenburger, R., von Gunten, L., Urrutia, R., Fischer, D., Fujak, M., Hamann, Y., Greber, N.D., Grosjean, M., 2013. Late Holocene air temperature variability reconstructed from the sediments of Laguna Escondida, Patagonia, Chile (45°30′S). *Palaeogeography, Palaeoclimatology, Palaeoecology*. 369, 482–492. https://doi.org/10.1016/j.palaeo.2012.11.013

Fontijn, K., Lachowycz, S.M., Rawson, H., Pyle, D.M., Mather, T.A., Naranjo, J.A., Moreno-Roa, H., 2014. Late Quaternary tephrostratigraphy of southern Chile and Argentina. *Quaternary Science Reviews*. 89, 70–84. https://doi.org/10.1016/j.quascirev.2014.02.007

Fontijn, K., Rawson, H., Van Daele, M., Moernaut, J., Abarzúa, A.M., Heirman, K., Bertrand, S., Pyle, D.M., Mather, T.A., De Batist, M., Naranjo, J.A., Moreno, H., 2016. Synchronisation of sedimentary records using tephra: A postglacial tephrochronological model for the Chilean Lake District. *Quaternary Science Reviews*. 137, 234–254. https://doi.org/10.1016/j.quascirev.2016.02.015

Futa, K., Stern, C.R., 1988. Sr and Nd isotopic and trace element compositions of Quaternary volcanic centers of the Southern Andes. *Earth and Planetary Science Letters*. 88, 253–262. https://doi.org/10.1016/0012-821X(88)90082-9

Gutiérrez, F., Gioncada, A., González Ferran, O., Lahsen, A., Mazzuoli, R., 2005. The Hudson Volcano and surrounding monogenetic centres (Chilean Patagonia): An example of volcanism associated with ridge – trench collision environment. *Journal of Volcanology and Geothermal Research*. 145, 207–233. https://doi.org/10.1016/j.jvolgeores.2005.01.014

Haberle, S.G., Lumley, S.H., 1998. Age and origin of tephras recorded in postglacial lake sediments to the west of the southern Andes, 44°S to 47°S. *Journal of Volcanology and Geothermal Research*. 84, 239–256. https://doi.org/10.1016/S0377-0273(98)00037-7

Hogg, A.G., Hua, Q., Blackwell, P.G., Niu, M., Buck, C.E., Guilderson, T.P., Heaton, T.J., Palmer, J.G., Reimer, P.J., Reimer, R.W., Turney, C.S.M., Zimmerman, S.R.H., 2013. SHCal13 Southern Hemisphere Calibration, 0–50,000 Years cal BP. *Radiocarbon* 55, 1889–1903. https://doi.org/10.2458/azu_js_rc.55.16783

Kratzmann, D.J., Carey, S., Scasso, R., Naranjo, J.-A., 2009. Compositional variations and magma mixing in the 1991 eruptions of Hudson volcano, Chile. *Bulletin of Volcanology*. 71, 419–439. https://doi.org/10.1007/s00445-008-0234-x

Kratzmann, D.J., Carey, S., Scasso, R.A., Naranjo, J.A., 2010. Role of cryptic amphibole crystallization in magma differentiation at Hudson volcano, Southern Volcanic Zone, Chile. *Contributions to Mineralogy and Petrology*. 159, 237–264. https://doi.org/10.1007/s00410-009-0426-1

López-Escobar, L., Cembrano, J., Moreno, H., 1995a. Geochemistry and tectonics of the Chilean southern Andes basaltic Quaternary volcanism (37-46°S). *Revista Geológica de Chile* 22, 219–234. 10.5027/andgeoV22n2-a06

López-Escobar, L., Kilian, R., Kempton, P.D., Tariri, M., 1993. Petrography and geochemistry of Quaternary rocks from the Southern Volcanic Zone of the Andes between 41°30'and 46°00'S, Chile. *Revista Geológica de Chile* 20, 33–55.

López-Escobar, L., Parada, M.Á., Hickey-Vargas, R., Frey, F.A., Kempton, P.D., Moreno, H., 1995b. Calbuco Volcano and minor eruptive centers distributed along the Liquiñe-Ofqui Fault Zone, Chile (41°-42° S): contrasting origin of andesitic and basaltic magma in the Southern Volcanic Zone of the Andes. *Contributions to Mineralogy and Petrology*. 119, 345–361. https://doi.org/10.1007/BF00286934

Lowe, D.J., 2011. Tephrochronology and its application: A review. *Quaternary Geochronology*. 6, 107–153. https://doi.org/10.1016/j.quageo.2010.08.003

Markgraf, V., Whitlock, C., Haberle, S., 2007. Vegetation and fire history during the last 18,000 cal yr B.P. in Southern Patagonia: Mallín Pollux, Coyhaique, Province Aisén (45°41′30″ S, 71°50′30″ W, 640 m elevation). *Palaeogeography, Palaeoclimatology, Palaeoecology*. 254, 492–507. https://doi.org/10.1016/j.palaeo.2007.07.008

McCulloch, R.D., Figuerero Torres, M.J., Mengoni Goñalons, G.L., Barclay, R., Mansilla, C., 2017. A Holocene record of environmental change from Río Zeballos, central Patagonia. *The Holocene* 27, 941–950. https://doi.org/10.1177/0959683616678460

Miranda, C.G., Vilanova, I., Moreno, P.I., Villa-Martínez, R., 2013. Glacial fluctuations in the Coyhaique-Balmaceda sector of central Patagonia (45°S-46°S) during the last glacial termination. *Bollettino di Geofisica Teorica e Applicata*. 54, 268–271.

Moreno, P.I., Francois, J.P., Moy, C.M., Villa-Martínez, R., 2010. Covariability of the Southern Westerlies and atmospheric CO2 during the Holocene. *Geology* 38, 727–730. https://doi.org/10.1130/G30962.1

Naranjo, J.A., Stern, C.R., 1998. Holocene explosive activity of Hudson Volcano, southern Andes. *Bulletin of Volcanology*. 59, 291–306. https://doi.org/10.1007/s004450050193

Naranjo, J.A., Stern, C.R., 2004. Holocene tephrochronology of the southernmost part (42°30' - 45°S) of the Andean Southern Volcanic Zone. *Revista Geológica de Chile* 31, 225–240. https://doi.org/10.4067/S0716-02082004000200003

Rawson, H., Naranjo, J.A., Smith, V.C., Fontijn, K., Pyle, D.M., Mather, T.A., Moreno, H., 2015. The frequency and magnitude of post-glacial explosive eruptions at Volcán Mocho-Choshuenco, southern Chile. *Journal of Volcanology and Geothermal Research*. 299, 103–129. https://doi.org/10.1016/j.jvolgeores.2015.04.003

Rawson, H., Pyle, D.M., Mather, T.A., Smith, V.C., Fontijn, K., Lachowycz, S.M., Naranjo, J.A., 2016. The magmatic and eruptive response of arc volcanoes to deglaciation: Insights from southern Chile. *Geology* 44, 251–254. https://doi.org/10.1130/G37504.1

Rodríguez, C., Sellés, D., Dungan, M., Langmuir, C., Leeman, W., 2007. Adakitic dacites formed by intracrustal crystal fractionation of water-rich parent magmas at Nevado de Longaví volcano (36.2°S; Andean Southern Volcanic Zone, Central Chile). *Journal of Petrology*. 48, 2033–2061. https://doi.org/10.1093/petrology/egm049

Saadat, S., Stern, C.R., 2011. Petrochemistry and genesis of olivine basalts from small monogenetic parasitic cones of Bazman stratovolcano, Makran arc, southeastern Iran. *Lithos*. 125, 607–619. https://doi.org/10.1016/j.lithos.2011.03.014

Sellés, D., Rodriguez, C.A., Dungan, M.A., 2004. Geochemistry of Nevado de Longavi Volcano (36.2S): a compositionally atypical arc volcano in the Southern Volcanic Zone of the Andes. *Andean Geology*. 31, 293–315. https://doi.org/10.4090/juee.2008.v2n2.033040

Stern, C., de Porras, M.E., Maldonado, A., 2015. Tephrochronology of the upper Río Cisnes valley (44°S), southern Chile. *Andean Geology*. 42, 173–189. https://doi.org/10.5027/andgeoV42n2-a02

Stern, C., Moreno, P.I., Henríquez, W.I., Villa-Martínez, R., Sagredo, E., Aravena, J.C., De Pol-Holz, R., 2016. Holocene tephrochronology around Cochrane (~47° S), southern Chile. *Andean Geology*. 43, 1–19. https://doi.org/10.5027/andgeoV43n1-a01

Stern, C.R., 2004. Active Andean volcanism: its geologic and tectonic setting. *Revista Geológica de Chile* 31, 1–51. https://doi.org/10.4067/S0716-02082004000200001

Stuiver, M., Reimer, P.J., Braziunas, T.F., 1998. High-Precision Radiocarbon Age Calibration for Terrestrial and Marine Samples. *Radiocarbon* 40, 1127–1151. https://doi.org/10.2458/azu_js_rc.v40i3.3786

Van Daele, M., Bertrand, S., Meyer, I., Moernaut, J., Vandoorne, W., Siani, G., Tanghe, N., Ghazoui, Z., Pino, M., Urrutia, R., De Batist, M., 2016. Late Quaternary evolution of Lago Castor (Chile, 45.6°S): Timing of the deglaciation in northern Patagonia and evolution of the southern westerlies during the last 17 kyr. *Quaternary Science Reviews*. 133, 130–146. https://doi.org/10.1016/j.quascirev.2015.12.021

Vargas, G., Rebolledo, S., Sepúlveda, S.A., Lahsen, A., Thiele, R., Townley, B., Padilla, C., Rauld, R., Herrera, M.J., Lara, M., 2013. Submarine earthquake rupture, active faulting and volcanism along the major Liquiñe-Ofqui Fault Zone and implications for seismic hazard assessment in the Patagonian Andes. *Andean Geology*. 40. https://doi.org/10.5027/andgeoV40n1-a07

Völker, D., Kutterolf, S., Wehrmann, H., 2011. Comparative mass balance of volcanic edifices at the southern volcanic zone of the Andes between 33°S and 46°S. *Journal of Volcanology and Geothermal Research* 205, 114–129. https://doi.org/10.1016/j.jvolgeores.2011.03.011

Watt, S.F.L., Pyle, D.M., Mather, T.A., 2013. The volcanic response to deglaciation: Evidence from glaciated arcs and a reassessment of global eruption records. *Earth-Science Reviews*. 122, 77–102. https://doi.org/10.1016/j.earscirev.2013.03.007

Watt, S.F.L., Pyle, D.M., Mather, T.A., 2011a. Geology, petrology and geochemistry of the dome complex of Huequi volcano, southern Chile. *Andean Geology*. 38, 335–348. https://doi.org/10.5027/andgeoV38n2-a05

Watt, S.F.L., Pyle, D.M., Naranjo, J.A., Rosqvist, G., Mella, M., Mather, T.A., Moreno, H., 2011b. Holocene tephrochronology of the Hualaihue region (Andean southern volcanic zone, ~42° S), southern Chile. *Quaternary International* 246, 324–343. https://doi.org/10.1016/j.quaint.2011.05.029

Weller, D.J., de Porras, M.E., Maldonado, A., Mendez, C., Stern, C.R., 2017. Holocene tephrochronology of the lower Río Cisnes valley, southern Chile. *Andean Geology*. 44, 229–248. https://doi.org/10.5027/andgeoV44n3-a01

Weller, D.J., Miranda, C.G., Moreno, P.I., Villa-Martínez, R., Stern, C.R., 2015. Tephrochronology of the southernmost Andean Southern Volcanic Zone, Chile. *Bulletin of Volcanology* 77, 1–24. https://doi.org/10.1007/s00445-015-0991-2

Weller, D.J., Miranda, C.G., Moreno, P.I., Villa-Martínez, R., Stern, C.R., 2014. The large late-glacial Ho eruption of the Hudson volcano, southern Chile. *Bulletin of Volcanology* 76, 1–18. https://doi.org/10.1007/s00445-014-0831-9

Wright, H.E., 1967. A square-rod piston sampler for lake sediments. *Journal of Sedimentary Research* 37, 975–976. https://doi.org/10.1306/74D71807-2B21-11D7-8648000102C1865D